Mechanical confinement effects on the phase separation morphology of polymer blend thin films

K. Dalnoki-Veress, J. A. Forrest, and J. R. Dutcher*
Department of Physics and the Guelph-Waterloo Program for Graduate Work in Physics, University of Guelph, Guelph, Ontario, Canada N1G 2W1
(Received 28 October 1997)

We have measured the phase separation morphology of polystyrene–poly (methyl methacrylate) (PS-PMMA) blend films of thickness h on a silicon oxide (SiO_x) substrate with a SiO_x capping layer. We observe a novel phase separation morphology for small capping layer thicknesses L and a transition from lateral to lamellar morphology as L is increased. We present a simple model that explains the observed lateral morphology and the transition in morphology in terms of a balance between the free energy increase associated with forming the interfaces between PS-rich and PMMA-rich domains and the free energy increase associated with the elastic bending of the SiO_x capping layer. The simple model reveals the dependence of the transition capping layer thickness L_c on the polymer blend film thickness h, and gives a reasonable quantitative prediction of L_c. [S1063-651X(98)11505-2]

PACS number(s): 68.55.−a, 64.75.+g, 68.35.Bs, 36.20.−r

INTRODUCTION

The control of the patterns of atoms or molecules assembled on an underlying substrate is important in polymeric [1], biological [2], semiconductor [3], and magnetic [4] systems used in fundamental research and technological applications. The self-assembly of polymer molecules on a substrate can be controlled by selectively modifying the chemistry of the substrate surface and/or the polymers to create patterned polymer films with tailored length scales. Patterning of thin polymer blend films can also be achieved by the thermodynamically driven phase separation process.

The phase separation morphology [5–13] and dynamics [14–17] of thin polymer blend films have been studied extensively. Phase separation of spin-coated polymer blend films can occur during the spin-coating process for high molecular weight (M_w) polymers [5–7], or upon annealing for low M_w polymers [8–13]. For thin films, the presence of the film interfaces can affect the phase separation morphology dramatically. For example, the film interfaces can induce a modulation normal to the film plane in the concentration of each component of a binary polymer blend (surface-directed spinodal decomposition) [8] because of the preference of one of the constituent polymers for the film interfaces. The presence of a wetting layer can result in lamellar phase separation morphology, which has been observed for a variety of polymer blend systems [9–11]. The film interfaces can also influence the phase separation morphology produced during the spin-coating of very thin, high M_w polymer blends [5].

The topography of the upper surface of polymer blend films can also be modified by the phase separation process. Recent atomic force microscopy measurements of blend films with a free upper surface have revealed a roughening of the upper film surface that accompanies the formation of lateral, phase-separated domains [12,13]. This effect can be understood in terms of the interfacial and surface tensions [18].

In the present measurements, we investigate the effect of varying the degree of mechanical confinement of low M_w polystyrene–poly (methyl methacrylate) (PS-PMMA) blend films on the phase separation process. The blend films of thickness h are fully constrained on the lower film surface by an underlying silicon oxide (SiO_x) substrate, and the confinement of the upper film surface is varied by preparing samples with different thicknesses L of a SiO_x capping layer. Phase separation is allowed to proceed by heating the films above the glass transition temperature of both polymer components. For films that have been annealed for a long time, we observe a qualitative difference in the phase separation morphology for small and large values of L. Many long, parallel phase-separated domains are observed within the plane of the film for small values of L. This type of lateral morphology differs qualitatively from that observed for polymer blend films with a free upper surface [13]. For large values of L, a lamellar morphology is observed. We present a simple calculation that accounts for the free energy changes that occur during phase separation due to the interfacial tension between the two polymers and the elastic bending of the capping layer. Using this model, we can explain the nature of the lateral morphology for small L, which is necessarily accompanied by a deformation of the upper film surface. Also, the transition from lateral to lamellar morphology as L is increased can be both understood qualitatively and predicted quantitatively. We find that the period and amplitude of the deformation of the upper film surface can be controlled directly by varying h and L.

SAMPLE PREPARATION AND EXPERIMENTAL DETAILS

The substrates were prepared by evaporating a 70 nm layer of SiO_x onto a clean Si(001) wafer (1 cm×1 cm). To evaporate the SiO_x layer, SiO powder was placed in a baffled tantalum boat (R.D. Mathis Co. model ME 1). The SiO powder was heated in vacuum to 100 °C for ~12 h to remove adsorbed impurities. The ambient pressure in the evaporator was 1×10^{-6} torr, and the pressure during the evaporation was $(1-2)\times10^{-5}$ torr. The deposition rate used was 0.5

*Author to whom correspondence should be addressed.

nm/s as monitored using a 5.0688 MHz crystal oscillator (M-Tron model MTO-T1-S3), which was calibrated by measuring the final film thickness using an ellipsometer. Ellipsometry was also used to determine that the index of refraction of the SiO_x layers was consistent with a value of $1<x<2$.

After the preparation of the substrate, the PS-PMMA polymer blend film was deposited using spin coating. We used PS of molecular weight $\overline{M}_w = 24\,700$ and polydispersity index $\overline{M}_w/\overline{M}_n = 1.03$, and PMMA of molecular weight $\overline{M}_w = 19\,300$ and polydispersity index $\overline{M}_w/\overline{M}_n = 1.06$ [19]. The PS and PMMA polymers were dissolved in a common solvent of toluene, with the total polymer concentration of the solutions varied between 1.25% and 5.00% (by mass). A spin speed of 4000 rpm was used to deposit all films, which resulted in polymer blend film thicknesses ranging from 37 nm to 148 nm, as measured using ellipsometry. For all of the solutions used in this study, the PS volume fraction was chosen to be the critical volume fraction $\phi_c = 0.48$, as calculated using Flory-Huggins theory [21]. Following the deposition of the polymer blend films, the films were annealed for 10 h at $T = 70$ °C ($<T_g$ for both polymers) in vacuum to drive off residual solvent without allowing phase separation to proceed. The resulting polymer blend films were homogeneous on all length scales that can be accessed using optical microscopy (as small as 0.3 μm).

The polymer blend films were then capped by evaporating a layer of SiO_x of thickness L. Evaporation of SiO_x onto polymer films produces sharp polymer-SiO_x interfaces [20]. The capping layer provides some degree of mechanical confinement of the polymer blend films while ensuring that both sides of each polymer film are chemically similar. During the deposition of the capping layer care must be taken to avoid heating the sample significantly to avoid possible damage to the polymer blend film as well as to prevent phase separation from occurring in the polymer blend film. For the slow SiO_x evaporation rates that we used (~ 0.5 nm/s), the temperature of the sample did not exceed 70 °C during the deposition of the SiO_x capping layer. Following the deposition of the capping layer, each sample consisted of a homogeneous (on length scales larger than 0.3 μm) polymer blend film sandwiched between SiO_x layers. We prepared a total of 30 samples with the blend film thickness h ranging from 37 to 148 nm and the capping layer thickness L ranging from 20 to 101 nm.

To allow phase separation to occur within the homogeneous PS-PMMA blend films, the samples were heated quickly (quench time $t_Q \sim 10$ s) from room temperature to the annealing temperature $T_A = 125$ °C by placing them onto a metal plate held at temperature T_A within an oven. T_A is greater than T_g for both polymers. The film temperature was held at T_A for several minutes to allow phase separation to proceed and then the films were rapidly quenched to room temperature by removing them from the oven and placing them onto a metal plate held at room temperature. The quench time for cooling was comparable to t_Q. At room temperature, a high-resolution reflected light optical microscope coupled to a charge-coupled device camera was used to measure the phase-separation morphology. The temperature was cycled repeatedly between room temperature and T_A to track the time evolution of phase separation in the blend films.

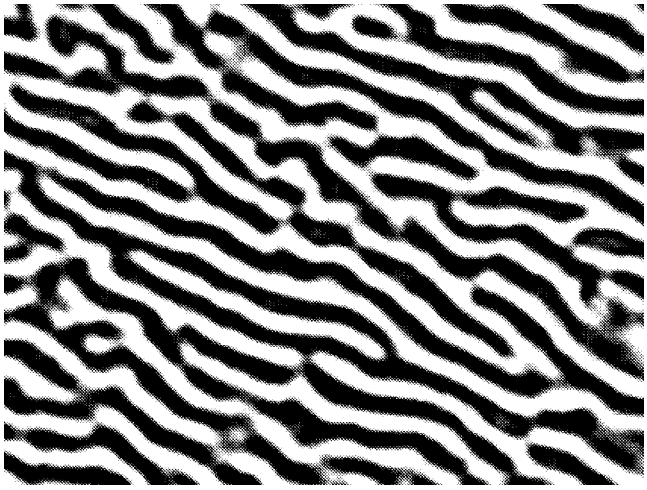

FIG. 1. Optical microscopy image (31.5 μm$\times$26.2 μm) of a PS-PMMA film with $h = 148$ nm and $L = 61$ nm showing lateral phase separation.

It was not necessary to use stains to enhance the optical contrast between the two polymer components since the difference in the index of refraction ($n_{PS} = 1.59$ and $n_{PMMA} = 1.49$) was sufficient to allow optical imaging of the morphology.

RESULTS AND DISCUSSION

After the films were annealed, two general types of phase separation morphology were observed. For small values of the capping layer thickness L, lateral phase separation was observed using optical microscopy. The lateral morphology consisted of many, randomly oriented regions, each of which contained a large numbnr of long, parallel domains with a well-defined periodicity within the plane of the film. A particularly good example of the parallel-domain morphology is illustrated in Fig. 1 for a PS-PMMA film with $h = 148$ nm and $L = 61$ nm which was annealed at $T_A = 125$ °C for 33 min. The domains are essentially interconnected because the PS volume fraction was chosen to be equal to the critical volume fraction $\phi_c = 0.48$. For the sample in Fig. 1, the domains have a characteristic width that is 1.2 ± 0.1 μm. We note that the in-plane domain widths (~ 1 μm) and the in-plane domain lengths ($\gg 1 \mu$m) are much larger than the thickness of the domains ($0.037 - 0.148$ μm) such that the domains are very nearly two dimensional. With successive annealing cycles, the domains were observed to grow until they reached a maximum size characterized by a width that was typically $0.5 - 1.5$ μm. In all cases, the growth of the domains was complete after 30 min of annealing time. The image shown in Fig. 1 was obtained after the domain growth was complete. Following the saturation of the domain size, no further changes in the morphology were observed with the films held at $T_A = 125$ °C for three days. Similar ''pinning'' of the phase separation morphology in thin polymer blend films has been observed previously [7,16] and is thought to be due to the existence of a long-lived, metastable state. In the present paper we focus on the final phase separation morphology achieved for each film, and the depen-

dence of this morphology on the polymer blend film thickness h and the capping layer thickness L. The time dependence of the phase separation morphology will be described in another publication [22].

For samples with L larger than a critical value L_c, lateral domains were not observed using optical microscopy, even for annealing times as long as three days. Since the PS-PMMA system must phase separate when heated above the T_g values of both components, a different type of phase-separation morphology must be obtained. Because of the differences in the PS-SiO_x and PMMA-SiO_x interactions, the blend films phase separate into a lamellar film structure with PMMA-rich layers in contact with SiO_x when heated above the T_g values of both components. We have verified the preference of PMMA for SiO_x experimentally through a series of dewetting experiments that show that thin films of the PMMA molecules on a Si substrate coated with a layer of SiO_x will not dewet when heated to $T=150$ °C, whereas thin films of the PS molecules on SiO_x will dewet completely after several hours at the same temperature. Therefore, for a PS-PMMA blend thin film with both surfaces in contact with SiO_x, PMMA will segregate to the SiO_x interfaces with the center of the film being PS rich. This type of lamellar phase separation has been observed previously [9–11].

We have demonstrated the existence of the lamellar phase-separation morphology directly by selectively removing each layer within the films using carefully chosen, selective solvents. It is imperative that each of the solvents remove the layer of interest without disturbing, i.e., removing or swelling, the underlying layers. We performed careful tests of a wide variety of solvents before deciding to use the following: a 10% solution of hydrofluoric acid in water to remove the SiO_x capping layer, glacial acetic acid to remove the PMMA-rich layer, and carbon tetrachloride to remove the PS-rich layer. Successive use of these solvents resulted in layer-by-layer removal of the film. For films with $L>L_c$, this simple procedure revealed the lamellar structure of the phase-separated polymer blend film by direct observation of a change in the color (and therefore thickness) of the film after each solvent was used.

For polymer blend films confined on both film surfaces by identical material, one might expect to obtain lamellar phase-separation morphology because of the preference of one of the constituent polymers for the confining material. In our measurements of PS-PMMA blend films between SiO_x layers, we observe lamellar morphology for large values of L, but for $L<L_c$, lateral domains are observed. Reducing L reduces the mechanical confinement of the top surface of the film, allowing the possibility of deformation of the top surface of the film. The deformation costs energy because of the elastic bending of the capping layer, which has two important consequences. First, deformations will not occur for a sufficiently thick capping layer. Second, for a thin capping layer, deformations will be restricted to parallel bends of the capping layer since parallel, in-plane bends cost less energy than deformations along nonparallel, in-plane directions (imagine, for example, bending a sheet of paper). By deforming a thin capping layer with parallel bends, a smaller surface-area-to-volume ratio is obtained for flattened cylindrical domains within the blend film (corresponding to lateral morphology) than for the central domain in a lamellar structure. The reduction in the surface-area-to-volume ratio corresponds to a reduction in the interfacial area between the two polymers and is energetically favored. Therefore, lateral domains will form within the blend films if the decrease of the free energy associated with the reduction in the interfacial area between the two polymers is greater than the increase in the free energy associated with the elastic bending of the capping layer. This gives a qualitative explanation of our experimental results: for $L>L_c$, we observe lamellar morphology, and for $L<L_c$, we observe parallel lateral domains (cf. Fig. 1).

To obtain a quantitative understanding of the dependence of the phase separation morphology on the thickness of the capping layer, we examine in more detail the change in the free energy ΔF associated with the phase separation process for a thin film sample. We take into account three different contributions to ΔF. First, there is a reduction in the free energy ΔF_ϕ associated with bulk phase separation, as determined using Flory-Huggins theory. This contribution is independent of the morphology and must be sufficiently negative to ensure that phase-separation occurs. The second term discussed above describes the free-energy increase ΔF_γ associated with forming the interfaces between PS-rich and PMMA-rich regions, and is given by the PS-PMMA interfacial tension multiplied by the total interfacial area between the domain and the matrix. The third term, also discussed above, describes the free-energy increase ΔF_b associated with the elastic bending of the SiO_x capping layer, which can occur during the phase-separation process. Assuming a periodic deformation along the x direction with amplitude A and wavelength λ, the bending energy for the entire sample is calculated to be [23]

$$\Delta F_b=\frac{EL^3}{24(1-\sigma^2)}\int_0^w\frac{l}{\lambda}\int_0^\lambda\left\{\frac{\partial^2}{\partial x^2}\left[A\cos\left(\frac{2\pi x}{\lambda}\right)\right]\right\}^2 dxdy$$
$$=\frac{KL^3A^2wl}{\lambda^4}, \tag{1}$$

where E and σ are the Young's modulus and Poisson's ratio of the capping layer material, l and w are the dimensions of the sample along the in-plane x and y directions, and K is given by a combination of the mechanical properties of the capping layer:

$$K=\frac{E\pi^4}{3(1-\sigma^2)}.$$

The quantity l/λ corresponds to the number of domains along the x direction. To account for surface effects in the thin films, we assume the presence of a thin wetting layer of PMMA-rich polymer next to the SiO_x layers, regardless of the morphology. This assumption is consistent with the results of the PS-SiO_x and PMMA-SiO_x dewetting experiments described above, and also with the observation of lamellar morphologies for similar systems [9–11].

In Fig. 2 we show a schematic diagram of the cross section of the film morphology for a film that exhibits lateral phase separation. This schematic diagram illustrates only one domain, i.e., one wavelength of the periodic deformation.

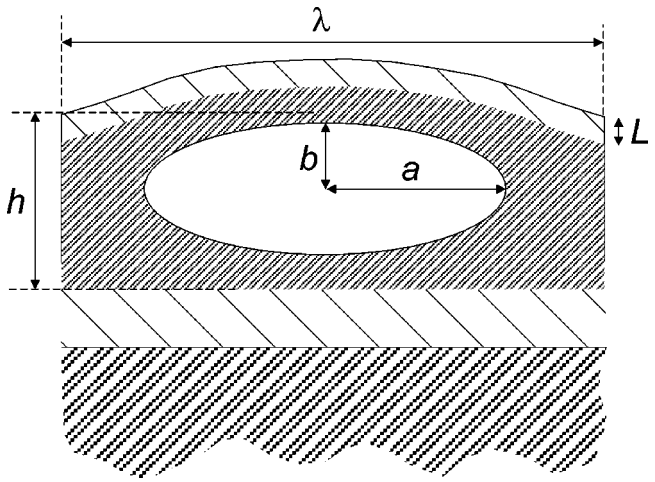

FIG. 2. Schematic diagram of the cross section of a single lateral domain, which illustrates the parameters used in the calculation (see text).

We assume that each domain in the sample extends infinitely in the y direction and that the domains are repeated with period λ in the x direction. For illustration purposes, we have represented the domain cross section in Fig. 2 as elliptical with the lengths of the semimajor and semiminor axes denoted by a and b, respectively. It is important to note that the calculation of L_c presented below is performed assuming *no* specific domain shape, only that the domain cross section is characterized by height $2b$, width $2a$, cross-sectional area A_d, and perimeter P_d. A specific domain shape is chosen only to relate the final calculated result to that measured experimentally.

The free energy ΔF_γ associated with the PS-PMMA interfacial tension is given by

$$\Delta F_\gamma = \gamma w \frac{l}{\lambda} P_d , \tag{2}$$

where γ is the PS-PMMA interfacial tension. Because the volume must remain constant, regardless of the aspect ratio of the domains, there is a constraint on the cross-sectional area of the domain A_d:

$$A_d = \frac{h\lambda}{(R+1)}, \tag{3}$$

where R is the ratio of the volume of the PMMA-rich region to that of the PS-rich region. For polymer blends of critical composition in which the constituent polymers have equal degrees of polymerization $R=1$. This is a good approximation for the experimental system described here.

The total change in the free energy per unit area $\Delta\mathcal{F}_{\rm lat}$ associated with phase separation into the lateral morphology is given by

$$\Delta\mathcal{F}_{\rm lat} = \frac{\Delta F_\gamma + \Delta F_b}{wl} = \frac{\gamma P_d}{\lambda} + \frac{KL^3A^2}{\lambda^4}, \tag{4}$$

where we have ignored the ΔF_ϕ term, which is constant and independent of the sample morphology. The total free energy per unit area $\Delta\mathcal{F}_{\rm lam}$ for phase separation into the lamellar morphology (two planar PS-PMMA interfaces) is simply given by $\Delta\mathcal{F}_{\rm lam} = 2\gamma$. We compare the free energy of the two final morphologies to determine which morphology is favored for a particular value of L. In the limit that $L \to 0$, $\Delta\mathcal{F}_{\rm lat} \to \gamma P_d/\lambda$ and the lateral morphology is obtained for $P_d < 2\lambda$. In the limit that L is large, $\Delta\mathcal{F}_{\rm lat}$ becomes large ($\sim L^3$) and the lamellar morphology is favored. The transition between lateral and lamellar morphology occurs for $\Delta\mathcal{F}_{\rm lat} = \Delta\mathcal{F}_{\rm lam}$, corresponding to the transition capping layer thickness L_c, which is given by

$$L_c = \left[\frac{\lambda^4 \gamma}{KA^2} \left(2 - \frac{P_d}{\lambda} \right) \right]^{1/3}, \tag{5}$$

with the perimeter P_d chosen such that A_d remain constant [see Eq. (3)].

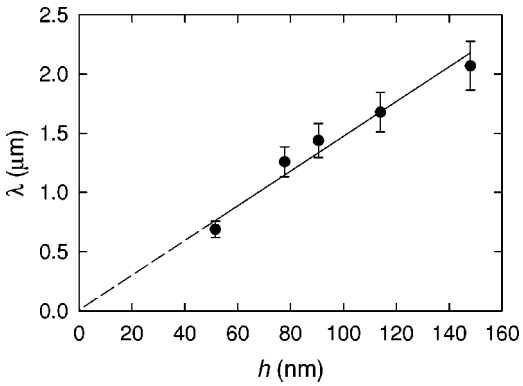

FIG. 3. Average wavelength λ vs the PS-PMMA blend film thickness h for films with L values equal to the largest value for which lateral phase separation was observed. The solid line represents a linear regression fit to the data: $\lambda = (14.7 \pm 0.5)h$.

Before the calculated values of L_c can be compared to those measured experimentally, it is necessary to specify the deformation wavelength λ. Our simple model does not predict a preferred value of λ; instead λ must be obtained from the experiment. For each h value, we choose the sample with the largest L value for which lateral phase separation is observed, corresponding to L less than but approximately equal to L_c. We find that the measured λ values for these samples depend linearly on the blend film thickness h for the range of h values studied, as shown in Fig. 3. A linear regression of the data for five different h values yields $\lambda = (14.7 \pm 0.5)h$.

The dependence of L_c on the film thickness h can be understood in terms of a scaling argument. Because of the observed linear dependence of λ on h for samples with L less than but approximately equal to L_c, as shown in Fig. 3, the cross-sectional area A_d of a domain scales like $A_d \sim h\lambda \sim h^2$. Since the domain area, as specified by its width $2a$ and its height $2b$ (see Fig. 2), can in general be written as $A_d = c_1a^2 + c_2b^2 + c_3ab$, where c_i are constants determined by the geometry of the domain shape, both a and $b \sim h$. It then follows that the domain perimeter $P_d \sim h$.

The scaling behavior of the deformation amplitude A is less trivial. The amplitude A must depend on the height of the domain $2b$ and can be written as

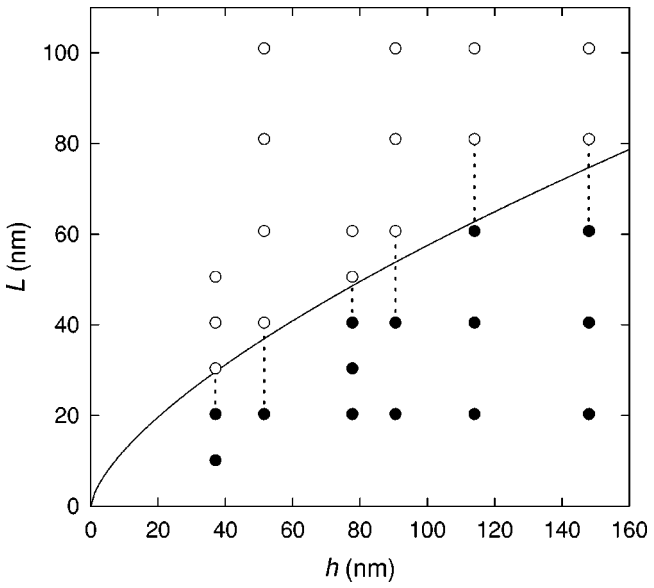

FIG. 4. Plot of the capping layer thickness L as a function of the PS-PMMA blend film thickness h for all of the samples used in the present study. The solid circles correspond to samples for which lateral morphology was observed, and the open circles correspond to samples for which lamellar morphology was observed. For each h value, dashed lines extend between the largest L value for which lateral morphology was observed and the smallest L value for which lamellar morphology was observed. The solid curve corresponds to calculated values of the transition capping layer thickness $L_c = \mathcal{C} h^{2/3}$, using the best fit value for $\mathcal{C} = 2.65 \pm 0.13$ nm$^{1/3}$.

$$A = \alpha \left[b - \frac{h}{2(R+1)} \right]^{\nu}, \tag{6}$$

where α is a proportionality constant and ν is the scaling constant. The square bracketed term in Eq. (6) ensures that the correct minimum value for b is obtained in the limit of no deformation (lamellar morphology). Since $b \sim h$, Eq. (6) implies that $A \sim h^{\nu}$. This scaling behavior for A combined with $\lambda \sim h$ and $P_d \sim h$ means that L_c, as specified by Eq. (5), scales like $L_c \sim h^{(4-2\nu)/3}$.

In Fig. 4 is shown a plot of the capping layer thickness L as a function of the polymer blend film thickness h for all of the samples used in the present study. Two different types of symbols are used: solid circles for samples for which lateral morphology was observed, and open circles for samples for which lamellar morphology was observed. For each h value, dashed lines extend between the largest L value for which lateral morphology was observed and the smallest L value for which lamellar morphology was observed. The transition between lateral and lamellar morphology occurs within the dashed range of L values.

A fit of the data in Fig. 4 to $L_c \sim h^{(4-2\nu)/3}$ gives the best fit value for the scaling parameter $\nu = 0.9 \pm 0.2$. The magnitude of ν can be understood from the following argument. If the height of the domain is increased by some factor then the deformation amplitude cannot increase by more than the same factor, since the deformation of the capping layer is the result of the increase in the domain height. This means that $\nu \leqslant 1$. Conversely, the height of the domain cannot increase with h much more quickly than the undulation amplitude, since the domain would not remain confined within the sample. Therefore, we expect that $\nu \sim 1$, which is consistent with the best fit value of $\nu = 0.9 \pm 0.2$. As a convenient approximation that is not expected to be rigorously true but that is consistent with the experimental results, we take $\nu = 1$. This is equivalent to assuming constant wetting layer thickness both above and below the domain for small deformations. The solid line in Fig. 4 corresponds to a least squares fit of the data to the relation $L_c = \mathcal{C} h^{2/3}$, where the best fit value for the prefactor is $\mathcal{C} = 2.65 \pm 0.13$ nm$^{1/3}$. Clearly, the solid curve is a good fit to the data since the solid curve passes through the dashed lines for all h values.

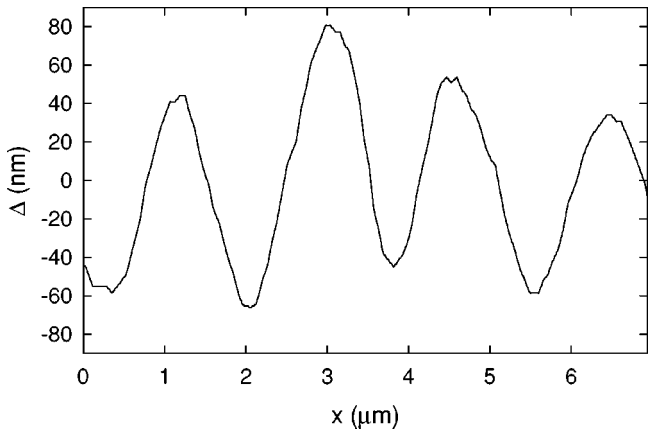

FIG. 5. Surface profile of the same PS-PMMA film as in Fig. 1 ($h = 148$ nm and $L = 61$ nm) measured using atomic force microscopy. The profile was collected along the direction normal to several long, parallel lateral domains. The average of the surface profile amplitude values Δ has been chosen to be zero.

Having established the scaling behavior of L_c with h it is also possible to compare the best fit value of the prefactor $\mathcal{C}$ to the value obtained from measurements of the morphology of a specific sample for which lateral phase separation was observed with L less than but approximately equal to L_c. For this comparison, we consider the sample with $L = 61$ nm and $h = 148$ nm (see Fig. 4). The deformation amplitude A for this sample was measured directly using atomic force microscopy (AFM). In Fig. 5 is shown a typical AFM trace of the surface profile across several domains. The profile is well described as sinusoidal, which is consistent with the calculation of the free energy increase ΔF_b associated with the elastic bending of the capping layer described above, and the average amplitude of many (>10) such profiles is $A = 30 \pm 5$ nm. The average deformation wavelength λ measured using optical microscopy is $\lambda = 2.1 \pm 0.2$ μm, and the average domain width is $2a = 1.2 \pm 0.1$ μm.

Using the AFM and optical microscopy data, we can calculate the prefactor $\mathcal{C}$ by specifying the material properties of the sample and choosing a specific shape for the cross section of the domains. For the material properties we choose capping layer Young's modulus $E = 72$ GPa and Poisson's ratio $\sigma = 0.16$ [24], PS-PMMA interfacial tension (at 125 °C) $\gamma = 1.83$ dyne/cm [25], and $R = 1$. The E and σ values are the bulk parameters for fused quartz (amorphous SiO_2). For the shape of the domain cross section, we consider two choices: the simple case of an ellipse as illustrated in Fig. 2, and the more realistic shape corresponding to con-

stant wetting layer thickness both above and below the domain (flat on the bottom and sinusoidal on the top, with the top and bottom surfaces of the domain joined by semicircular arcs). In each case, the perimeter P_d is calculated under the constraint of Eq. (3). For both choices of domain cross-section shape, we obtain the same value, $\mathcal{C} = 0.86$ nm$^{1/3}$, which is in reasonable agreement (approximately a factor of three) with the best fit value of $\mathcal{C}$. The lack of sensitivity of $\mathcal{C}$ to the specific choice of domain shape occurs because the only aspect of the domain shape that determines L_c is the perimeter P_d, and P_d is virtually identical for different reasonable choices of the domain shape since $a \gg b$ for $L \sim L_c$.

The agreement between the prefactor $\mathcal{C}$ values obtained by fitting the data in Fig. 4 and that calculated from the direct measurement of the deformation amplitude is quite remarkable given the simple nature of the model and the fact that we have taken the mechanical properties of the SiO_x capping layer to be those of amorphous SiO_2. Another aspect not taken into account in this simple model is the contribution of dispersion forces [26]. For the changes in morphology observed in this study the contribution of dispersion to the change in the free energy is at least four orders of magnitude smaller than that due to interfacial tension.

The calculation of the transition between lateral and lamellar phase separation as the capping layer thickness L is increased is based on comparing the free energies of the two possible final morphologies. We have also minimized the free energy of the lateral morphology with respect to the domain shape parameter b [the other domain shape parameter a is determined through the volume fraction constraint given by Eq. (3)]. In this second approach, the transition from lateral to lamellar morphology occurs for the capping layer thickness for which neighboring domains touch: $2a = \lambda$. Although the two approaches are conceptually quite different with regard to the process by which the sample undergoes phase separation, the difference between the result of the two approaches is small: the scaling properties are identical and the prefactor differs by less than 35% for the samples used in the present study.

SUMMARY AND CONCLUSIONS

We have presented the results of measurements of the phase separation morphology of PS-PMMA blend films on a SiO_x substrate with a SiO_x capping layer. We find that there is a qualitative change in the phase separation morphology as the capping layer thickness L is increased. The lateral phase separation morphology obtained for small values of L consists of many long, parallel domains. The transition from lateral to lamellar morphology with increasing L can be explained using a simple model that accounts for the free energy increase associated with forming the interfaces between the PS-rich and PMMA-rich domains and the free energy increase associated with the elastic deformation or bending of the capping layer. The simple model reveals the dependence of the transition capping layer thickness L_c on the polymer blend film thickness h, and gives a reasonable quantitative prediction of L_c. For samples that exhibit lateral phase separation, direct control of the amplitude and period of the deformation is achieved by varying h and L.

ACKNOWLEDGMENTS

We thank Dr. B. G. Nickel for many useful discussions, Dr. M. W. Matsen for his comments on the original manuscript, which led to a simplification of the calculation, Dr. D. Thomas for the use of his AFM, C. Gigault for help with the AFM measurements, and Waterloo Digital Electronics for the use of their EXACTA 2000 ellipsometer. The financial support of the Natural Sciences and Engineering Research Council (NSERC) of Canada is gratefully acknowledged.

[1] A. C. Balazs, C. Singh, E. Zhulina, D. Gersappe, and G. Pickett, MRS Bull. **22**, 16 (1997).
[2] J. T. Groves, N. Ulman, and S. G. Boxer, Science **275**, 651 (1997).
[3] D. E. Jesson, K. M. Chen, and S. J. Pennycook, MRS Bull. **21**, 31 (1996).
[4] E. D. Dahlberg and J.-G. Zhu, Phys. Today **48**(4), 34 (1995).
[5] K. Dalnoki-Veress, J. A. Forrest, J. R. Stevens, and J. R. Dutcher, J. Polym. Sci., Part B: Polym. Phys. **34**, 3017 (1996).
[6] K. Dalnoki-Veress, J. A. Forrest, J. R. Stevens, and J. R. Dutcher, Physica A **239**, 87 (1997).
[7] S. Walheim, M. Böltau, J. Mlynek, G. Krausch, and U. Steiner, Macromolecules **30**, 4995 (1997).
[8] R. A. L. Jones, L. J. Norton, E. J. Kramer, F. S. Bates, and P. Wiltzius, Phys. Rev. Lett. **66**, 1326 (1991).
[9] F. Bruder and R. Brenn, Phys. Rev. Lett. **69**, 624 (1992).
[10] M. Georghegan, R. A. L. Jones, R. S. Payne, P. Sakellariou, A. S. Clough, and J. Penfold, Polymer **35**, 2019 (1994).
[11] M. Georghegan, R. A. L. Jones, and A. S. Clough, J. Chem. Phys. **103**, 2719 (1995).
[12] K. Tanaka, A. Takahara, and T. Kajiyama, Macromolecules **29**, 3232 (1996).
[13] T. M. Slawecki, A. Karim, S. K. Kumar, T. P. Russell, S. K. Satija, C. C. Han, Y. Liu, M. H. Rafailovich, J. Sokolov, R. M. Overney, and S. A. Schwarz (unpublished).
[14] G. Krausch, C.-A. Dai, E. J. Kramer, and F. S. Bates, Ber. Bunsenges. Phys. Chem. **98**, 446 (1994).
[15] C. K. Haas and J. M. Torkelson, Phys. Rev. Lett. **75**, 3134 (1995); C. K. Haas and J. M. Torkelson, Phys. Rev. E **55**, 3191 (1997).
[16] L. Sung, A. Karim, J. F. Douglas, and C. C. Han, Phys. Rev. Lett. **76**, 4368 (1996).
[17] H. Tanaka, Phys. Rev. Lett. **76**, 787 (1996).
[18] P. Keblinski, S. K. Kumar, A. Maritan, J. Koplik, and J. R. Banavar, Phys. Rev. Lett. **76**, 1106 (1996).
[19] Polymer samples were obtained from Polymer Source Inc.
[20] P. Lambooy, J. R. Salem, and T. P. Russell, Thin Solid Films **252**, 75 (1994).
[21] P. J. Flory, *Principles of Polymer Chemistry* (Cornell University Press, Ithaca, 1953).

[22] K. Dalnoki-Veress, J. A. Forrest, and J. R. Dutcher (unpublished).
[23] L. D. Landau and E. M. Lifshitz, *Theory of Elasticity*, 3rd ed. (Pergamon Press, Oxford, 1986), pp. 38–40.
[24] *CRC Handbook of Chemistry and Physics*, edited by D. R. Lide, 75th ed. (CRC Press, Boca Raton, 1994).
[25] *Polymer Handbook*, edited by J. Brandrup and E. H. Immergut, 3rd ed. (Wiley, New York, 1989).
[26] J. N. Israelachvili, *Intermolecular & Surface Forces*, 2nd ed. (Academic Press, San Diego, 1991).